Eur. J. Mineral.
2008, **20**, 673–685
Published online August 2008

The combined influence of mineralogical, hygric and thermal properties on the durability of porous building stones

DAVID BENAVENTE[1, 2, *], GIUSEPPE CULTRONE[3] and MIGUEL GÓMEZ-HERAS[4]

[1]Departamento de Ciencias de la Tierra y del Medio Ambiente, Universidad de Alicante, Alicante, Spain
*Corresponding author, e-mail: david.benavente@ua.es
[2]Laboratorio de Petrología Aplicada, Unidad Asociada CSIC-UA, Alicante, Spain
[3]Departamento de Mineralogía y Petrología, Facultad de Ciencias, Universidad de Granada, Granada, Spain
[4]School of Geography, Archaeology and Palaeoecology, Queen's University Belfast, Belfast, UK

Abstract: It is a common practice to test building stones against an isolated decay factor when assessing the durability of building stones. Accordingly, the interpretation of results is often driven by the considerations of a limited number of properties thought as relevant to the action of that specific decay factor. In this way, the role of the synergies of decay processes and agents is often neglected. Contrarily, when different decay factors are included in the same experiment and the stone properties are examined conjunctly, the difficulties of isolating the effects of a specific decay factor or of isolating the contribution of ''relevant'' stone properties become apparent.

The aim of this paper is to assess the combined contribution of mineralogical, hygric and thermal properties to the durability of different stones after exposure to laboratory-simulated cyclic decay combining wetness and temperature variations. For this purpose, 10 stone types were selected to emphasize the impact of the mineralogical heterogeneity on stone decay, in particular the coexistence of calcareous and siliceous grains and the occurrence of clays. The results emphasize the importance of considering the relations between decay factors and highlight how stone properties must be considered as a whole in order to assess and understand the durability of building stones.

Key-words: stone decay, durability test, hygric dilatation, thermal expansion, clay minerals.

Introduction

Stone decay can be defined as the result of environmental change from a stone in equilibrium state in the lithosphere to its exposure to radically different conditions in the atmosphere, hydrosphere and/or biosphere (Aires Barros, 2002). This definition highlights the importance of changing environments, and therefore changes in the equilibrium between stone and environment, as decay drivers for stone. In this sense, decay factors that are naturally cyclic count among the most important threats to stone. Water and heat are therefore considered some of the most important decay factors as they act cyclically, and their action can be detected even at the shortest frequencies through changes in wetness and temperature.

One of the main contexts where stone decay becomes highly relevant is in the built environment because of the enormous expenditure generated yearly for its restoration and maintenance, in addition to the cultural loss undergone in the context of stone-built Cultural Heritage. As a result of this, understanding the behaviour of stone in the environment and, eventually, predicting the type, pace and extent of decay is one of the main priorities for the scientific community. Nevertheless, stone decay is in many cases difficult to predict due to the large number of associated variables (Price, 1996; Prikryl *et al*., 2004). In addition to the difficulty of predicting the environmental patterns of change, especially considering the present context of uncertainty due to ongoing climate change, there is a tendency in laboratory simulation of testing the effects of isolated decay factors on the stone. In this way, the role of the combination of decay processes and the synergies between decay factors is often neglected. Also, the heterogeneity of many stone types used in construction increases the complexity of the assessment of their durability. This is especially noticeable in stones containing minerals susceptible to reacting in the presence of water, as for example clay minerals.

Moisture and water circulation in porous stones are widely recognised as a relevant decay factor for porous stone (*e.g.* Kühnel, 2002). Water will generate more or less accentuated decay depending on the chemical and mineralogical composition of the stone (Franzini *et al*., 2007). Clay minerals are common components of the clastic fraction of sedimentary stones and they are among the most susceptible to change in the presence of water. This is a result of their peculiar crystalline structure that can include water molecules within the lattice. The interaction between clay and water can favour aggregation–disaggregration or swelling–contraction

DOI: 10.1127/0935-1221/2008/0020-1850
0935-1221/08/0020-1850 $ 5.85

processes of clayey particles (Veniale *et al*., 2001) inducing deformations inside the stone and, therefore, reducing the stone's resistance to total breakdown (Delgado Rodrigues, 2001). Identifying the presence of clays is not enough when analyzing stone decay. In addition to this, the identification of the specific mineral phases present is necessary, since some types (*e.g.* smectites) are more susceptible than others to swelling when interacting with water (Sebastián *et al*., 2008).

Cyclic temperature changes are generally assumed to drive stone decay through the temperature gradients generated within the stone and the thermal expansion mismatch between minerals (*e.g.* Halsey *et al*., 1998; Weiss *et al*., 2004). Although the assumption of temperature fluctuations causing decay when applied as an isolated agent through so-called "insolation weathering" is to date still contentious (Gómez-Heras *et al*., 2006), temperature is also important because it influences on other factors that control decay as, for example, evaporation (Smith, 1977). In this sense, there is evidence of the influence of heating regimes and temperature changes on other decay factors, such as wetting and drying or salt crystallisation (Koch & Siegesmund, 2004; Gómez-Heras & Fort, 2007).

Therefore, the combined action of decay factors should be considered when planning and interpreting laboratory-simulated durability tests. There has been substantial progress recently on the consideration of the importance of the combination of decay factors and processes (McCabe *et al*., 2007a and b), but this is still not the norm in the studies of stone decay.

Under the light of these considerations, this paper explores the implications of the combination of water saturation and temperature changes as decay factors on the durability of a range of sedimentary stones used as building stones. The stone types used for this study were selected to stress the importance of the mineralogical heterogeneity as an additional factor influencing the stone decay; in particular, the coexistence of calcareous and siliceous grains and the occurrence of clays.

Materials and methods

Stone types

Ten types of porous stones were chosen in this study on the basis of their different lithological, petrographical and petrophysical characteristics. These were also selected as they are commonly used as building materials in different regions of Spain, in recent buildings and/or the built heritage. The stones tested (Table 1) range over four types of sandstones which contain different main grains or allochems: calcite (C), quartz–calcite (QC), quartz (Q) and dolomite (D).

Calcareous sandstones (C) are well-sorted biocalcarenites rich in foraminifers (mainly *Globigerinae*) ranging in size from 0.2 to 0.5 mm. Foraminifera shells are generally filled by glauconite and/or siliceous cement. The terrigenous fraction is comprised of quartz, feldspars, micas, dolostone and other rock fragments. Both interparticle and intraparticle porosity vary. The most abundant type of cement present in these stones is equant-equicrystalline mosaics of calcite spar. The biocalcarenites C2, C3, C4 and C5 have been widely used in the built heritage, and named respectively as Piedra Bateig Fantasía, Piedra Bateig Azul, Piedra Bateig Llana and Piedra Bateig Blanca (Fort *et al*., 2002).

Quartzose limestones or biomicrites (QC) contain foraminifers (mainly *Globigerinae*), ranging in size from 0.1 to 0.2 mm. The terrigenous fraction is mainly comprised of quartz, feldspars and micas. QC shows intraparticle and vuggy porosity.

Quartz sandstones (Q) present a variable quartz concentration. Q1 is a well-sorted quartz–arenite that consists of monocrystalline quartz grains with rare feldspars, metamorphic clasts, chert and muscovite grains. Primary interparticle porosity has been partially filled by silica cements that form frequent overgrowths on quartz grains (Benavente *et al*., 2007a). Q2 and Q3 can be classified as subarkoses or subfeldespathic arenites; they present in a high concentration of quartz, while feldspars, calcite and phyllosilicates (mostly chlorite and muscovite) appear in smaller amounts. The quartz crystals are angular to subrounded in shape. They are surrounded by feldspars (partially altered to sericite), phyllosilicates and an interparticle calcareous matrix that appears in sparse, unevenly distributed amounts. Quartz, feldspar and some phyllosilicate grains are around 350 μm in size. Sandstones Q2 and Q3 have also been used in the built heritage, named as Piedra Tarifa Dorada and Piedra Tarifa Gris, respectively (Sebastián *et al*., 2008).

The dolomitic sandstone (D) is a well-sorted sandstone consisting mainly of dolomite and calcite grains (Table 1). Detrital quartz grains and clay minerals are minor constituents of the sandstone. The ortochem is mesocrystalline calcite cement. Interparticle porosity is very abundant (Benavente *et al*., 2007a).

Mineralogy and texture

To identify the mineral phases in the different stone types, X-ray diffraction analyses were performed using a Philips PW-1710 diffractometer with automatic slit, Cu $K\alpha$ radiation (λ = 1.5405 Å), 40 kV, 40 mA, 3 to 60° 2θ explored area for the whole samples and 3 to 30° 2θ for the clay fraction and 0.01° 2θ s^{-1} goniometer speed. Samples were milled in an agate mortar to < 40 μm particle size, and then analysed. Interpretation of data was carried out using XPowder computer program (Martín Ramos, 2004).

The clay fraction (< 2 μm) was separated in ground samples by Stoke's law related methods. A mixture of hydrogen peroxide (20 vol. %) and distilled water was used to dissolve the organic material present if any. In Ca-rich samples, acetic acid (up to 1 N concentration) was used to remove carbonates. Samples were then deflocculated by repeated washing with distilled water. Following this, 5 g L^{-1} sodium hexametaphosphate was added to water to deflocculate the particles. Finally, the clay fraction was separated with a Kubota KS-8000 centrifuge and, subsequently, smeared on glass slides. An XRD analysis of the clay fraction was performed using orientated aggregates: air-dried,

Table 1. Results of XRD analysis of the whole samples and the fraction with < 2 μm grain size.

Sample	Whole sample						Clay fraction		
	Qtz	Phy	Dol	Cal	Pl	Interstr.	Sm	Ill	Chl
C1	*		*	***	tr		**	**	
C2	*			***	tr		**	**	
C3	*		*	***	tr		**	**	*
C4	*		*	***	tr		**	***	
C5	*		*	***	tr		**	**	
QC	**	*	*	**			**	**	*
Q1	***	tr							
Q2	***	tr		*	**	**		**	*
Q3	***	tr		*	*	**		*	**
D	tr		***	*	tr				

Qtz = quartz; Phy = phyllosilicates; Dol = dolomite; Cal = calcite; Pl = plagioclase; Sm = smectite; Ill = detrital mica; Chl = chlorite; Interstr = mixed layer chlorite + smectite; tr = trace; * = scarce; ** = abundant; *** = very abundant.

Table 2. Connected porosity, ϕ(Hg), pore volume, V_p(Hg) and mean pore radius, r_M, obtained by mercury intrusion porosimetry; specific surface area, SSA and pore volume, $V_p(N_2)$, obtained by nitrogen adsorption; bulk, ρ_{bulk}, and grain, ρ_{grain}, density; total porosity ϕ_T; capillary absorption coefficient, C; hygric swelling, $\Delta l/l_0$, of the stones.

Sample	ϕ(Hg) (%)	V_P(Hg) (cc g^{-1})	r_M (μm)	SSA (m^2 g^{-1})	$V_P(N_2)$ (cc g^{-1})	ρ_{bulk} (g cm^{-3})	ρ_{grain} (g cm^{-3})	ϕ_T (%)	C (kg m^{-2} h$^{-0.5}$)	$\Delta l/l_0$ (mm m^{-1})
C1	16.86	0.078	0.18	10.16	0.007	2.09	2.69	22.15	20.83	0.568
C2	15.65	0.073	0.33	9.85	0.018	2.17	2.72	20.05	20.83	–
C3	14.31	0.065	0.08	10.22	0.017	2.26	2.7	16.25	14.33	0.750
C4	18.83	0.093	1.48	8.42	0.013	2.11	2.72	22.26	41.33	0.186
C5	14.18	0.064	0.15	12.25	0.024	2.26	2.71	16.80	20.50	0.373
QC	26.02	0.134	0.35	12.69	0.016	1.97	2.71	27.09	35.00	1.639
Q1	13.48	0.059	2.43	2.31	0.004	2.28	2.67	14.62	28.00	0.067
Q2	18.43	0.080	0.17	9.93	0.011	2.09	2.71	22.87	14.83	0.978
Q3	7.39	0.030	0.38	4.95	0.007	2.37	2.7	12.39	12.83	0.325
D	19.52	0.096	6.71	0.69	0.001	2.22	2.8	20.46	140.00	0.202

solvated for 48 h at 60 °C with ethylene-glycol (Bruton, 1955) and heated for 1 h at 550 °C (Moore & Reynolds, 1989).

Semiquantitative analysis of mineral phases was performed converting the data to the constant sample volume and using the PDF2 database and Normalized Relative Intensity Ratio method (Table 1).

The clay distribution and microtexture of the stones were studied with a Leo Gemini 1530 field emission scanning electron microscopy (FESEM) coupled with Oxford INCA 200 microanalysis. FESEM secondary electron (SE) images were taken on 5 × 5 × 3 mm samples.

Porous media characterisation

Mercury intrusion porosimetry (MIP), nitrogen absorption technique and helium pycnometry were used to characterise the porous media of the studied building stones.

Connected porosity, ϕ(Hg), pore volume, V_p(Hg) and pore-size distribution, by means of median pore size (r_M), were obtained from MIP with an Autopore IV 9500 Micrometrics mercury porosimeter (Table 2). The pore-size interval characterisation by MIP ranges from 0.002 to 200 μm, which corresponds respectively to highest and lowest head pressures.

Nitrogen absorption technique (Autosorb-6 Quantachrome apparatus) was used to complete the micro-mesopore analysis (Fig. 1). The pore analysis was described in terms of pore-size distribution, pore volume, $V_p(N_2)$ and specific surface area (SSA). The determination of the SSA was carried out through the BET method in the relative pressure interval P/P_0 = 0.05–0.2. The pore-size distribution was obtained in the 0.0009–0.015 μm pore-size (radius) interval using the non-local density functional theory for N_2 at 77 K on silica.

Total porosity (ϕ_T) was calculated as follows:

$$\phi_T\,(\%) = \left(1 - \frac{\rho_b}{\rho_t}\right) \cdot 100, \qquad (1)$$

where ρ_t is the true density which is defined as the ratio of its mass to solid volume. True density was obtained by an AccuPyc 1330 Helium pycnometer. The dry bulk density, ρ_{bulk}, of a stone is defined as the ratio of its mass to its volume, including the volume of voids and grains (Table 2).

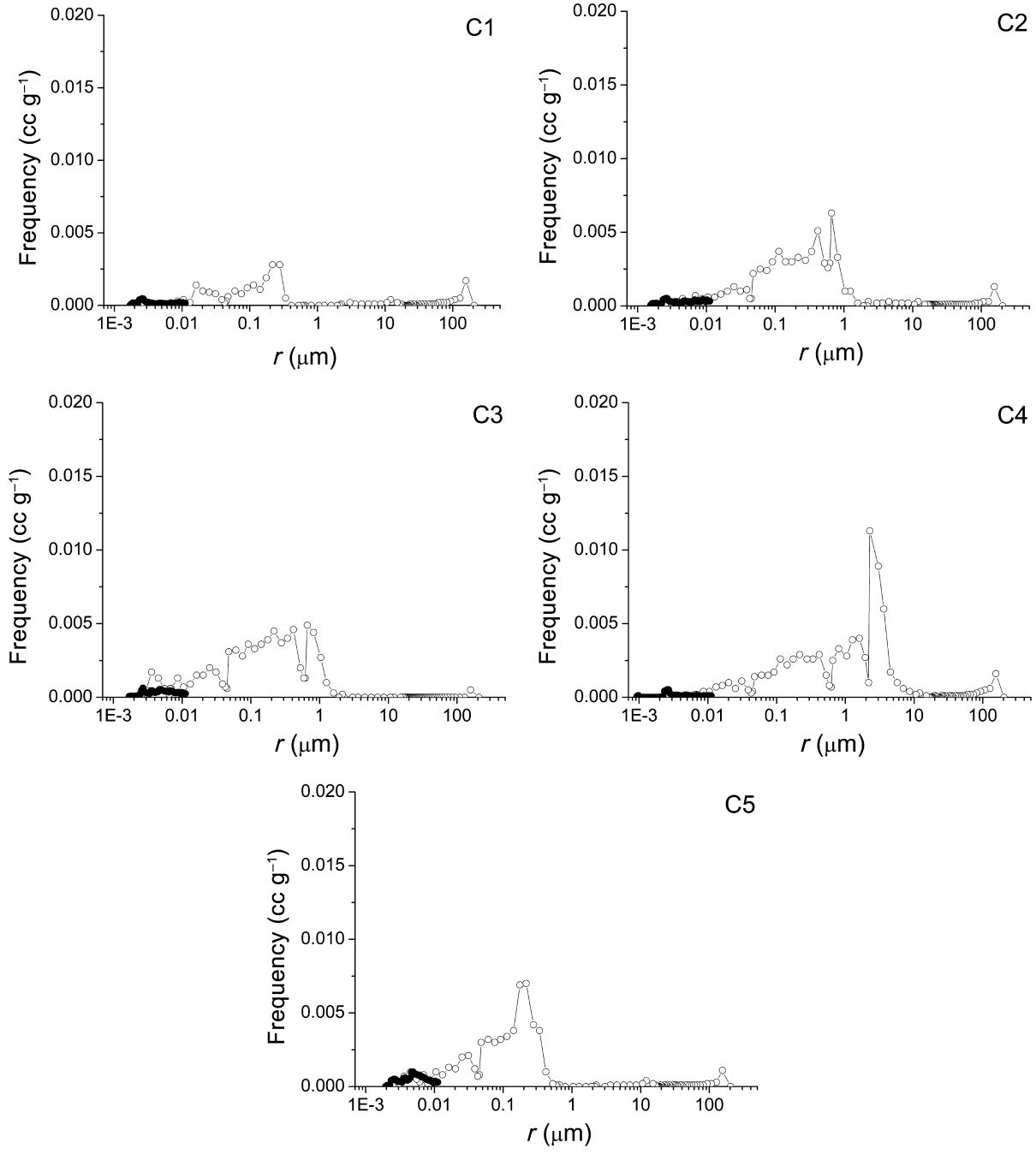

Fig. 1. Pore-size distribution curves of the stones obtained by nitrogen adsorption (close circles) and mercury intrusion porosimetry (open circles).

Hygric properties

The capillary water absorption was carried out using a weigh scale with continuous data-logging. The scale was connected to a computer which, through the software CK®, automatically records weight gain in the tested specimen at specific intervals (every 30 s for the current study). It allows automatic monitoring of the water uptake by the sample when its lower surface is in contact with the water reservoir (Benavente *et al*., 2007a). The results were plotted as absorbed water per area of the sample during imbibition *versus* the square root of time. Through this kind of representation, the capillary imbibition kinetic defines both the initial capillary absorption and then the saturation. The slope of the curve during capillary absorption is the capillary absorption coefficient, *C* (Table 2). This flow mechanism can be quantified by the capillary absorption coefficient, *C*, which is very much linked to the characteristics of both the pore structure and the fluid (Dullien *et al*., 1977; Hammecker & Jeannette, 1994; Benavente *et al*., 2002) and also related

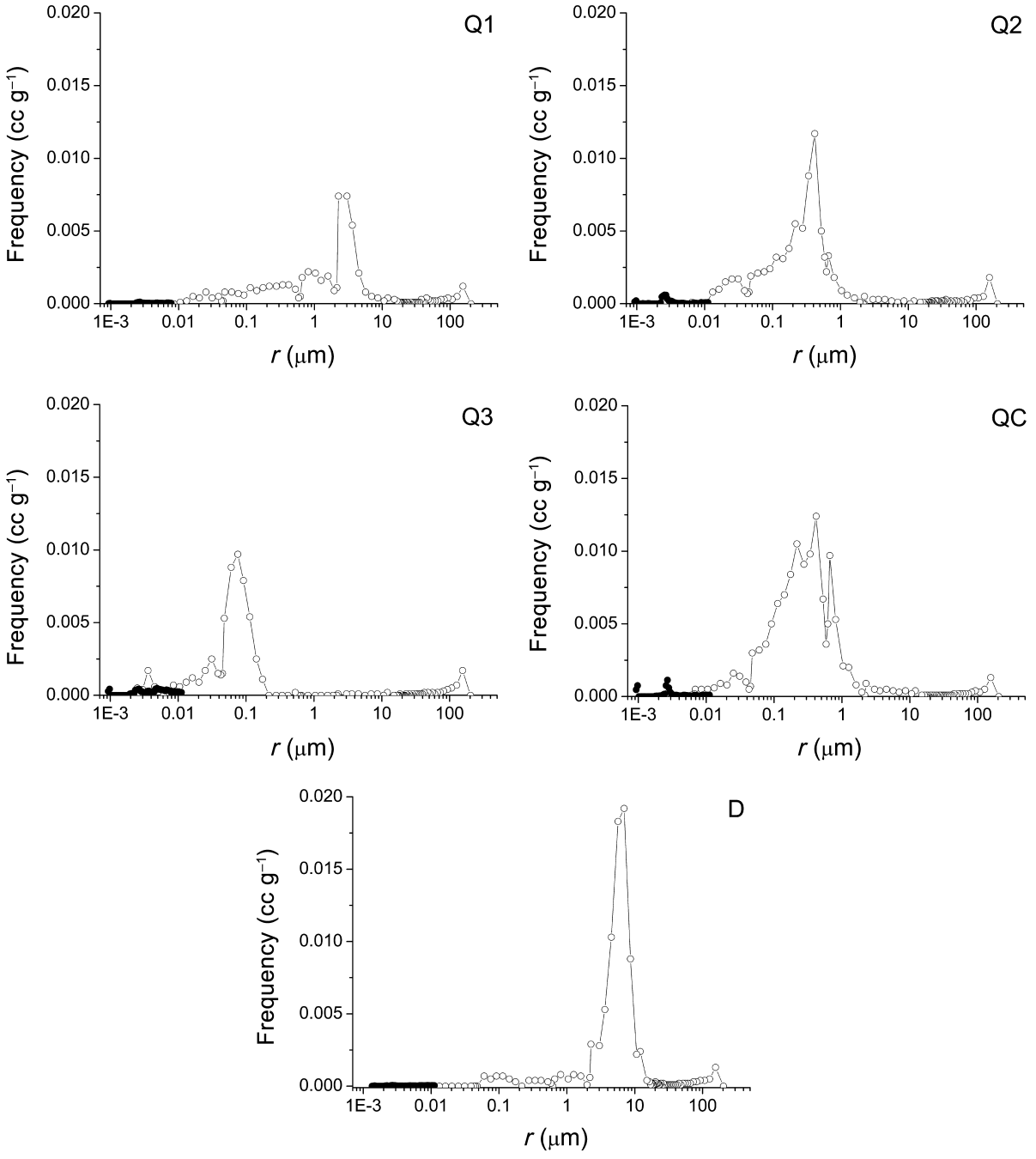

Fig. 1. continued.

to the square root of the permeability (Zimmerman & Bodvarsson, 1991; Benavente *et al*., 2007a).

The hygric swelling was measured at room temperature (20 °C) on ~ 10 × 10 × 30 mm samples. Three samples were submerged in water except for a small section to allow degasification and capillary water uptake. The vertical deformation was quantified with a Sensorex LVDT-SX8 displacement sensor (±1 μm resolution) which recorded the displacement value every 5 s. The hygric expansion was obtained as the maximum value of the vertical deformation per initial length, $\Delta l/l_0$ (Table 2).

Thermal properties

The thermal dilatation coefficient and thermal conductivity of the samples were measured to characterise the thermal properties of the building stones. The hysteresis in the thermal response curves was also evaluated.

Each sample was subjected to three heating–cooling cycles to characterise the thermal behaviour of the stones. A thermomechanical analyser (TMA Q400, TA Instruments) was used to obtain the thermal response curves from which the coefficient of thermal expansion was derived. Measurements

Table 3. Coefficient of linear expansion, α; thermal conductivity, k; compressional, v_P, and shear, v_S, wave velocities; dynamic Poisson ratio, ν; dynamic Young's modulus, E; uniaxial compressive strength, σ_C; and percentage of dry weight loss, ΔW, porosity, $\Delta\phi$, and compressional wave velocity, Δv_P, after wetting and drying durability test of the stones.

Sample	α (10^{-6} K^{-1})	k (W mK^{-1})	v_P (m s^{-1})	v_S (m s^{-1})	ν	E (GPa)	σ_C (MPa)	ΔW (%)	$\Delta\phi$ (%)	Δv_P (%)
C1	5.168	8.6	3780	2220	0.24	25.48	37.29	0.67	1.80	9.13
C2	4.957	6.6	4080	2614	0.15	34.18	27.9	0.49	0.81	3.89
C3	5.584	8.3	4029	2477	0.2	33.24	35.5	0.71	1.12	7.71
C4	6.662	7.4	3920	2377	0.21	28.87	23.5	0.51	0.62	4.63
C5	4.840	6.9	4008	2472	0.19	32.93	34.3	0.49	0.76	3.99
QC	5.644	6.5	2845	1770	0.19	14.7	4.27	0.96	2.51	10.76
Q1	11.901	10.4	4232	2765	0.13	39.27	67.8	0.05	0.65	0.82
Q2	8.598	5.0	2778	1718	0.18	14.62	14.41	0.53	0.70	5.85
Q3	7.420	–	2994	1918	0.15	19.95	33.08	0.51	1.25	5.02
D	7.360	8.3	4017	2546	0.16	33.58	33.5	0.24	0.99	0.44

were carried out on three ~ 10 mm cubes that were used using an applied force of 0.05 N, under nitrogen atmosphere, and in the temperature range 35–90 °C. Heating and cooling was performed with a velocity of 0.5 °C min^{-1} as representative of the average heating and cooling rate for a south-facing stone surface (data after Gómez-Heras, 2006) and to ensure thermal equilibration of the specimen.

Thermal conductivity, k, is the property of the material that indicates the heat flux through the material for a temperature gradient (Table 3). Thermal conductivity was measured with a relative steady-state technique. Three ~ 10 × 10 × 40 mm samples were placed between a water-cooled block and a reference glass sample, which is, in turn, connected to a hot water thermally stabilized bath. Losses through radiation and convection are neglected. The temperature gradient in the reference and in the sample is measured by three and two thermocouples, respectively. Thus, linearity in the reference also can be assessed, being typically within ±1 % (Molina *et al*., 2008).

The thermal dilatation coefficient, α (in 10^{-6} K^{-1}), was calculated according to:

$$\alpha = \frac{\Delta l / l_0}{\Delta T}, \tag{2}$$

where Δl is the length change of the sample, l_0 is the initial sample length and ΔT is the temperature interval (Table 3).

The hysteresis in the thermal cycle was calculated as the strain difference between the heating and cooling ramps for a given temperature. The hysteresis in the thermal cycles is very sensitive to the experimental conditions, particularly to the heating and cooling rates, sample size and shape, the period of time elapsed between the point at which the maximum temperature was reached; and the initiation of cooling (Arpon *et al*., 2003). Therefore, for the scope of this paper, hysteresis is used just as a qualitative parameter to understand the thermal behaviour of the studied stones.

Strength characterisation

Stone strength was characterised by uniaxial compressive and ultrasonic tests. The uniaxial compressive strength test is used to determine the maximum value of stress attained before failure. In the characterisation tests, six 70 mm cubes were used and the load rate was 0.36 kN s^{-1} (Table 3). The tests were carried out in accordance with the standard UNE-EN 1926 (Anon., 1999).

The ultrasonic measurements were carried out by means of the transmission method, which consists of two piezoelectric sensors coupled to the sample at constant pressure. Compressive (P) and shear (S) waves were measured using polarised Panametric transducers (500 kHz) and a Sonic Viewer-170, which acquired and digitalized the waveforms to be displayed, manipulated and stored (Table 3). Visco-elastic couplants were used to achieve good coupling between the transducer and the sample. The P-wave signal was recorded using an ultrasound eco-gel, whereas the S-wave signal was enhanced by using a normal incidence couplant (SWC, shear wave couplant, GE Panametrics®).

The dynamic elastic constants of the stones were calculated from the known ultrasonic wave velocities and bulk density, using the theory of elasticity (*e.g.* Christensen, 1990; Guéguen & Palciauskas, 1994; Tiab & Donaldson, 1996) (Table 3). Thus, the Poisson ratio, ν, and Young's modulus, E, were calculated as follows:

$$\nu = \frac{(v_P/v_S)^2 - 2}{2\left[(v_P/v_S)^2 - 1\right]}, \tag{3}$$

$$E = \rho_{bulk} v_P^2 \frac{(1-2\nu)(1+\nu)}{(1-\nu)}. \tag{4}$$

Wetting–drying and thermal durability tests

Three 25 × 25 × 40 mm samples for each stone type were subjected to 100 wetting–drying and heating–cooling cycles. Each of the cycles (24 h) consisted of a wetting and drying phase followed by a heating and cooling phase. In each cycle, samples were covered with distilled water at 20 °C for 16 h. Then, the samples were taken out of the water and introduced into an oven at 70 °C for 5 h. Finally, the samples were left for 3 h to cool to room temperature

(20 °C). Decay was quantified by the percentage of dry weight loss after the durability tests (ΔW (%)), the variation of connected porosity ($\Delta\phi$ (%)) and stone strength (Δv_P (%)) (Table 3).

Results and discussion

Tables 2 and 3 display the results obtained for each of the tests carried out and the parameters selected to assess the degree of decay after the durability tests. Despite the relatively small number of cycles, the differences between the tested stone types after the durability tests were noticeable. These differences reflect the influence of the petrophysical properties and microstructure of each of the stone types. The results show weight loss, a reduction in mechanical strength and a porosity increase for all the tested samples as a result of laboratory durability tests.

The quantification of stone breakdown with variation of weight loss, porosity and compressional wave velocity after durability test shows the same tendency regarding durability (Table 3). Weight loss is widely used as the sole indicator of deterioration in standard durability tests. However, for this type of building stone, its application may be highly restrictive as it only reflects the variable and superficial loss of material without measuring the internal reduction in stone strength, which is not visible in hand specimen. It was also reported that incomplete quantification of stone breakdown resulted from using weight loss for experimental weathering studies in, respectively, arenaceous and calcareous stones (Nicholson, 2001) and dolostones (Benavente *et al.*, 2007b).

In this study, the weight loss is used as an indicator of deterioration, since the goal is to link intrinsic stone properties to thermal and hygric deterioration. However, the variation of compressional wave velocity seems to be the most sensitive parameter to quantify stone deterioration, and therefore it should be considered pertinent for a more thorough assessment of decay.

In order to assess the relative influence of each of the stone properties on the decay experienced during the durability tests, a principal component analysis (PCA) was performed to simplify the number of variables to be compared. Once the main correlations were identified through PCA, several bivariate scatter diagrams were plotted for a focused study of these variables.

Principal component analysis

The PCA grouped the parameters considered in the database in three principal components (PC) which accounted for 92.5 % of the total variance (Table 4). The calculations were carried out using SPSS® v.14.0 code. PC1 links pore structure, mechanical properties and hygric and thermal expansions to the wetting–drying weathering, quantified by weight loss after the durability test, and accounts for 61.8 % of the total variation. Thus, in general terms, this relation indicates that stones with large pores; low values of porosity, SSA and hygric swelling; and strong mechanical properties are the most durable. Moreover, PC1 shows that there is a moderate positive correlation between coefficient of linear thermal expansion and weight loss after durability testing of the stones, which contrarily means that a porous stone subject to large thermal expansion is more durable. PC2 accounts for 19.9 % of the total variation and is associated with capillary water transport and pore structure. Finally, PC3 accounts for 10.8 % of the total variation and presents a moderate link between the coefficient of linear thermal expansion and compressional wave velocity.

Table 4. Principal component analysis of petrophysical properties and durability.

Component	1	2	3
r_M (μm)	0.633	0.752	0.164
SSA ($m^2\ g^{-1}$)	−0.839	−0.501	0.159
ϕ_T (%)	−0.768	0.518	0.020
C ($kg\ m^{-2}\ h^{-0.5}$)	0.406	0.837	0.354
v_P ($m\ s^{-1}$)	0.859	−0.307	0.398
E (GPa)	0.916	−0.270	0.256
σ_C (MPa)	0.893	−0.366	−0.149
k ($W\ mk^{-1}$)	0.816	−0.216	0.083
α ($10^{-6}\ K^{-1}$)	0.557	0.171	−0.803
$\Delta l/l_0$ ($mm\ m^{-1}$)	−0.885	0.074	−0.124
ΔW (%)	−0.895	−0.163	0.305
% explained of the total variance	61.8	19.9	10.8

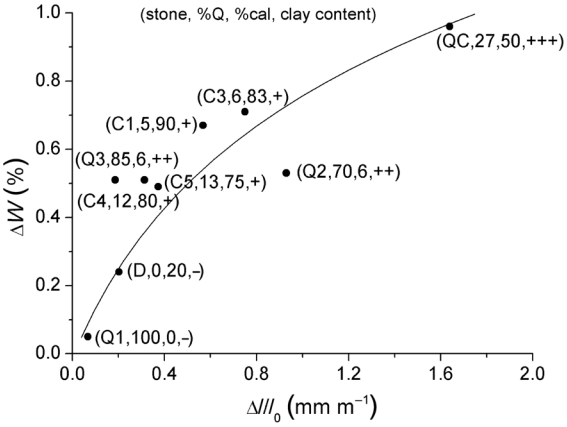

Fig. 2. Correlation between the percentage of weight loss by wet–dry weathering (ΔW) and hygric expansion ($\Delta l/l_0$). Quartz (%Q), calcite (%cal) and clay mineral content is shown in brackets. Clay fraction content is displayed as abundant (+++), medium (++), low (+) and absent (−).

Lithological heterogeneity: relations between clay content and hygric swelling

As the final analysis results, expressed as weight loss, show the best correlation with hygric swelling, this is to be considered the main factor accounting for stone decay. This mainly depends on two factors: mineralogical heterogeneity (most

noticeably the presence of clay minerals) (Table 1) and pore-size distribution (Fig. 1), as capillary forces may lead to relevant negative capillary pressures in micropores.

All samples swelled when saturated with water. The porous building stones show a large scattering of hygric expansion values (Fig. 2). Thus, while Q1 and D exhibit very small hygric swelling, Q2 and QC swell quite remarkably (Table 2). This shows a relation between the amount of clay minerals in the sample and hygric swelling. The latter samples present a high amount of interparticle clay minerals which lead to high degree of stone swelling and softening (Fig. 3a). An XRD orientated aggregates allowed us to detect the following clay minerals: detrital mica, smectite and low concentrations of chlorite and paligorskite, as well as a mixed layer made up of chlorite and smectite in the T1 and T2 samples (Table 1). According to Veniale *et al*. (2001), clays can undergo two types of expansion: (a) osmotic process (interparticle expansion) due to water molecules (and electrolytes in solution) adsorbed on the external surface of clay particles, and (b) intraparticle swelling produced by the interlayer expansion of the crystal-chemical units. The latter occurs only in "swelling minerals" like smectites. Therefore, smectites can experience both interparticle and intraparticle expansion simultaneously. Due to their smectite content, the QC, C1 and Q2 samples are the most damaged samples. The other non-expandable clay minerals can show interparticle expansion causing sandstones to suffer a progressive disintegration.

The interparticle clay minerals are usually found in the stone cement, binding the grains together. This type of binding phase increases their susceptibility to deterioration, especially under conditions of cyclic wetting and drying, causing swelling and shrinkage of clay minerals (Jiménez-González *et al*., 2008). Consequently, these clay minerals lead to a higher degree of decay in the stone due to their swelling and produce stone softening.

However, intraparticle clay minerals may produce swelling but not stone softening. FESEM observations identified small authigenic glauconite spherules in the calcareous sandstones (biocalcarenites) between grains and inside of foraminifer shells (Fig. 3b, c). It is important to mention that orientated aggregates diffractograms were unable to evaluate the displacement of the diffraction lines of glauconite after treatment with ethylene-glycol. According to Hower (1961), this mica usually contains up to a maximum of 10 % smectite-like expandable layers. Part of the glauconite is associated with foraminifer shells as intraparticle clay minerals. In these cases, although it may swell, this will not produce softening. Moreover, the intraparticle porosity within the foraminifers is not well-connected and, therefore, less accessible to water, so it reduces its relevance to the overall decay of the stone.

Q2 and Q3 present some sedimentary bedding recognizable by the basal planes of phyllosilicates (and clays) which are placed parallel to the stratification planes (Sebastián *et al*., 2008). The hygric expansion in the perpendicular direction was slightly higher than in the parallel direction. Similar behaviour in sedimentary bedding stones was also reported by Weiss *et al*. (2004).

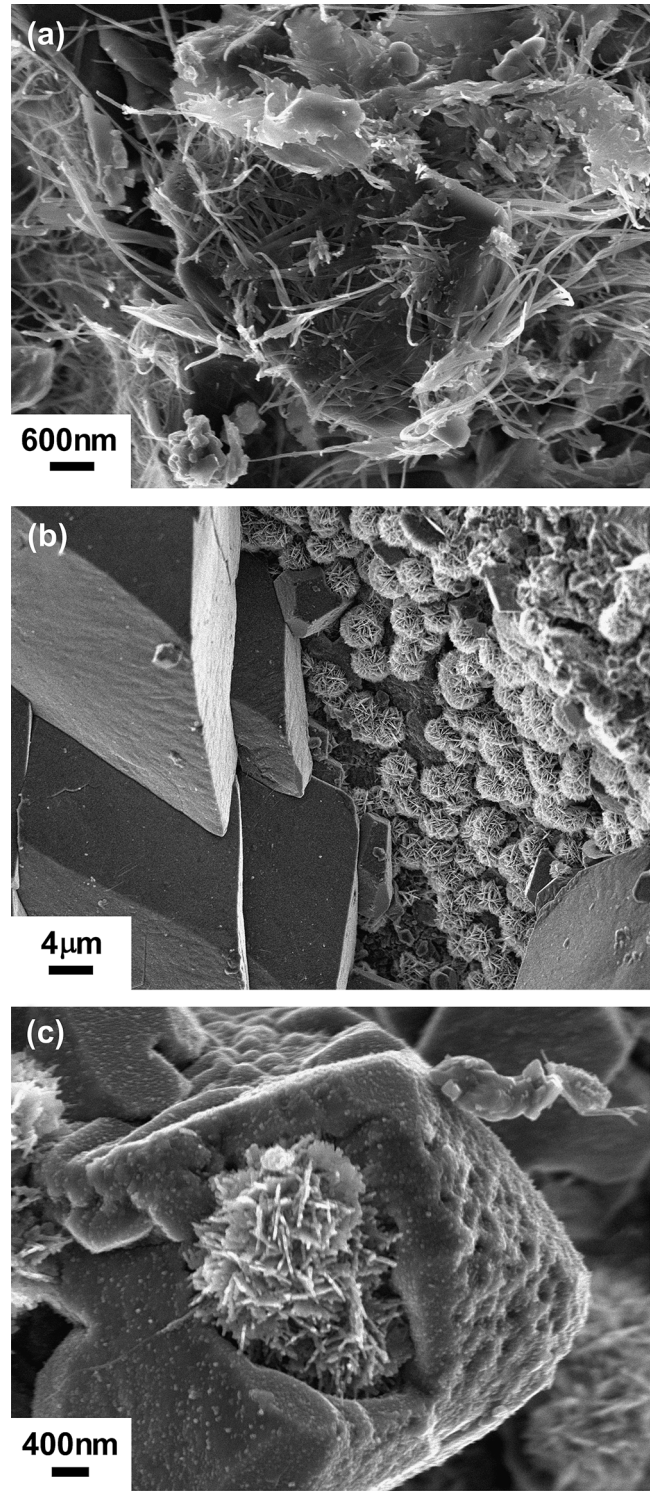

Fig. 3. FESEM micrographs and EXD analysis of sandstones were: (a) laminar (smectite) and fibrous (paligorskite) clay minerals can be recognized; (b) glauconite spherules (~ 2 μm in size) crystallize near calcite crystals; (c) development of glauconite inside a calcite grain.

Jiménez-González & Scherer (2004) point out that during the cycles of wetting and drying, stone damage might mainly take place during drying. During wetting, stone is

initially dry and then its surface gets wet. The wetted part will attempt to expand although it is constrained by the bulk of the dry block. In this case, the maximum stress occurs when the thin swelling layer is completely suppressed by the larger volume of dry stone. Thus, damage is expected to occur when this stress exceeds the compressive strength of the wet stone. On the contrary, when a wetted and expanded stone begins to dry from its surface, the drying layer will attempt to shrink. As the dimensional change is resisted by the bulk of the stone, the thin layer will be under a tensile stress. Thus, damage is expected when the stress exceeds the tensile strength of the dry stone. Stones generally have tensile strengths that are much lower than their compressive strengths, so damage should occur during the drying cycles. These decay processes can be enhanced if the stone is constrained. This situation is found in the built environment when, for example, stone blocks are confined by rigid mortar joints (Garrecht *et al*., 1996).

In addition to clays, there are other mineralogical/textural factors influencing the weight loss, including the compositional heterogeneity and the grain size of the stones. The results show a direct relation between weight loss and more complex mineralogical compositions of the stone. For example, QC and C3, which are the stones with more heterogeneous mineralogical composition, show the highest values of weight loss, while D and Q1, which are almost monomineral stones, show the lowest values of weight loss. Additionally, a trend relating stones with larger grain size to higher values of weight loss is also observed. Since these latter mineralogical and textural factors do not seem to show the same relation to hygric swelling as the clay content (Fig. 2), their contribution to stone decay is probably more related to the thermal properties of stone than to its hygric properties.

Pore structure and stone strength

Water produces hygric expansion when it invades the pore structure. On the contrary, when the pore liquid begins to evaporate, a meniscus develops in each pore such that the liquid goes into tension and creates compression within the stone. The capillary pressure in the pore liquid decreases (*i.e.* becomes increasingly negative) according to Laplace's equation:

$$\Delta p = \gamma_{LV}\,\kappa_{LV}, \tag{5}$$

where κ_{LV} is the curvature of the liquid–vapour meniscus in the pore entry and γ_{LV} is the interfacial energy between the liquid and vapour. If a meniscus with a wettable surface is supposed, Eq. (5) can be written for a cylindrical pore of radius r as:

$$\Delta p = -\frac{2\gamma_{SV}}{r}. \tag{6}$$

Capillary pressure can become important when porous stones have thin pores below 0.1 μm and are in advance stages of drying. As a consequence, hygric expansion and shrinkage cycles generate tension and compression episodes within the stone structure. Pejon & Zuquette (2002) point out this phenomenon as a common and important disaggregation mechanism in stone engineering because of the pressure developed which promotes swelling and breakdown of sedimentary stones (Seedsman, 1993). Eeckhout refers to this phenomenon as air breakage (Eeckhout, 1976).

This assertion explains the negative correlation after wetting–drying tests of weight loss (ΔW) and mean pore radius (r_M) as observed in PC1 (Table 4). Moreover, this component groups the durability with pore size, porosity and SSA. The latter is directly related to porosity and inversely related to pore size, so that it could be used to indicate stone's susceptibility to capillary pressure. Envisioning porous structure as a bundle of parallel capillary tubes, SSA is related to porosity and pore radius and as follows:

$$\mathrm{SSA} = \frac{2\phi}{\rho_{bulk}} \sum \frac{D_i}{r_i}, \tag{7}$$

where ρ_{bulk} is the bulk density and D_i is the normalized pore-size distribution. The SSA, therefore, includes pore structure information related to decay mechanisms. Thus, high SSA values mean that a greater surface area of the material will decay, implying a high susceptibility to salt weathering (Benavente *et al*., 2007a) and to capillary stress. High SSA values also indicate a high capacity and susceptibility to water condensation and retention within porous materials, and consequently, a high bioreceptivity (Sanchez-Moral *et al*., 2005).

The second component groups capillary water transport with pore structure. If a meniscus with a wettable surface is supposed, the capillary absorption coefficient, C, is related to pore radius and porosity as follows (Benavente *et al*., 2002; Mosquera *et al*., 2000):

$$C = \phi\rho\sqrt{\frac{r\gamma_{LV}}{2\eta}}, \tag{8}$$

where η is the water viscosity and ρ is the water density.

Results also show that stones with low compressive strength are the least durable, whilst those with high compressive strength are the most durable (Tables 3 and 4). The action of hygric expansion and shrinkage, combined with heating and cooling cycles, generates compression and tension episodes within the stone structure. Therefore, the higher the compressive strength, dynamic Young's modulus, and compressional wave velocity, the less susceptible the samples are to failing due to these episodes. This explains the inverse correlation between stone strength and weight loss after the wetting–drying test, as observed in PC1 (Table 4).

The importance of hygric swelling and stone strength on stone durability was also reported by Olivier (1979) who proposed a geodurability classification based on the free-swelling coefficient and uniaxial compressive strength. For example, according to Oliver's classification QC can be classified as a very poor stone; C3 as good, Q2 as fair; and Q1, Q3 and D as excellent.

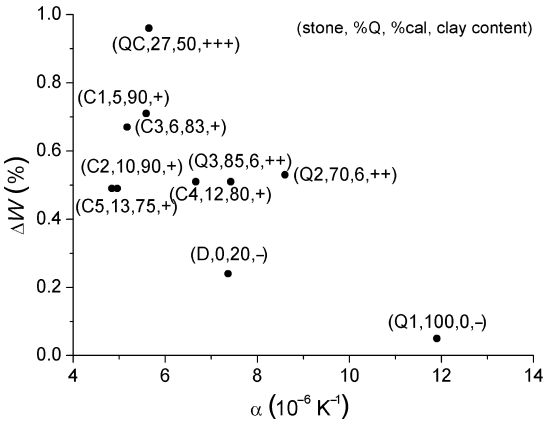

Fig. 4. Correlation between the percentage of weight loss by wet–dry weathering (ΔW), and coefficient of linear thermal expansion (α). Clay fraction content is displayed as abundant (+++), medium (++), low (+) and absent (−).

Influence of thermal properties

The stones display a wide range of thermal properties (Table 3). Results do not display a straightforward relation between thermal dilatation (α) and weight loss (ΔW) after decay tests (Fig. 4). Furthermore, PC1 shows a moderate negative correlation between α and ΔW (Table 4), which would mean, if interpreted simplistically, that porous stones with a higher thermal expansion coefficient will be less susceptible to decay.

This apparently contradictory relation highlights two main issues concerning the scale of observation in interpreting the influence of thermal properties on stone decay. Firstly, the effects of thermal properties on the decay of building stones are usually only observable on a longer-term basis through fatigue effects. Secondly, the differences of thermal properties at the individual mineral scale can enhance these processes (Gómez-Heras *et al*., 2006).

Therefore, on one hand, the relatively short length of these tests might have made the correlation between thermal properties and decay less noticeable. On the other hand, the stones present very heterogeneous mineralogical compositions and this has an effect on the observed decay patterns in terms of weight loss. The mineralogy of the stone and the relation between the adjacent minerals (texture) play an important role in controlling the thermal expansion of stones. The anisotropy of the linear expansion coefficient of minerals has an influence on the thermal behaviour of the entire stone, and the bulk thermal expansion of a stone does not necessarily reflect the processes of thermal expansion mismatch that happen at the individual mineral scale.

Calcite is a highly anisotropic mineral, whereas quartz has low anisotropy in relation to thermal expansion. However, the extraordinary anisotropic behaviour of calcite leads to relatively small volume expansion, as a random arrangement of crystallographic orientations within the stone generates random counteracting effects buffering the expansion of individual crystals. The opposite will occur with quartz and this explains the high thermal expansion of Q1, which is mainly constituted of quartz (Table 3).

In addition to this, the translation of the thermal expansion of individual minerals into bulk expansion of the stone is also buffered when the porosity is high and, therefore, there is more room within the stone for the thermal expansion to be accommodated. Moreover, the presence of clay minerals, which can act plastically, is also a competing factor to the expression of the individual grains thermal expansion into a bulk volume expansion of the stone.

Therefore, the bulk thermal expansion of a stone does not necessarily reflect its likeliness to undergo thermal-related decay and the analyses must take into account the differences at the mineral scale. The more heterogeneous the mineralogy of a stone, the greater is the likeliness of undergoing thermal decay through differences of thermal properties between the minerals. Different coexisting mineral phases with disparate thermal expansion responses enhance the thermal expansion mismatch between individual grains and may accelerate decay. Grain size heterogeneity is also mentioned as a factor enhancing thermal decay (Gómez-Heras *et al*., 2006).

This is observable in the above-mentioned correlation between weight loss and heterogeneous mineralogical composition of the stone. For example, QC and C3, which are the most heterogeneous stones, show the highest values of weight loss, whereas D and Q1, which are almost monomineral, show the lowest. Equally, it is observed that stones with larger grain size present higher values of weight loss.

In most cases, the thermal expansion curve for the dried samples is quite straight showing no hysteresis (Fig. 5). However, a small amount of hysteresis is found in C4, QC and Q2. Figure 5 compares the thermal expansion curves for clay-free stone (Q1) and clay-bearing stone (C4), which contains smectite and detrital mica. Although the hysteresis in the thermal response of the dried samples can be neglected, it must be considered in the future for a better understanding of the thermal behaviour of stones subjected to longer thermal experiments in wet conditions. For example, during the wetting–drying test, thermal expansion is produced when samples are wet. Koch & Siegesmund (2004) found a certain alteration of thermal expansion behaviour in saturated marbles. They proved marbles that show a large hygric expansion also show a linear increase in length due to temperature. This means that stones sensitive to hygric dilatation may also exhibit thermal expansion behaviour as a precursor. This process can also be enhanced by the presence of clay minerals (Fig. 4). As a consequence, moisture and temperature are observed to be linked both in the laboratory durability test and in the field.

Thermal conductivity values of the studied stones range from 5.0 to 10.4 W m^{-1} K^{-1}, as shown in Table 3. The thermal conductivity of the stone depends on several factors, including mineralogy and pore volume. In particular, quartz has a relatively high thermal conductivity, which explains why the highest value of 10.4 W m^{-1} K^{-1} was obtained from Q1 (100 % quartz). The results show a significant inverse correlation between thermal conductivity and weight loss. This inverse correlation reveals two things: on the one hand, the influence of porosity as a buffering agent for thermal decay, meaning the higher the porosity, the more

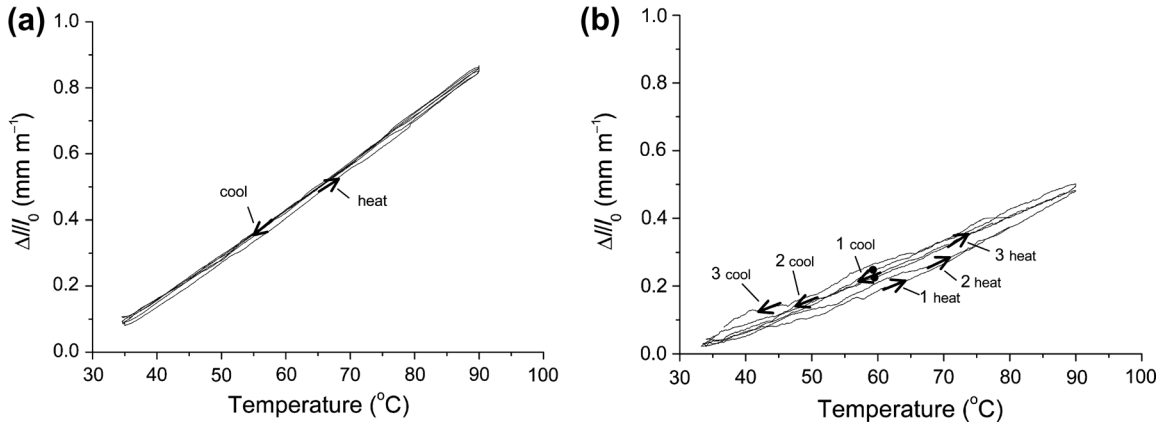

Fig. 5. Thermal expansion curves of quartz sandstone Q1 (a) and the calcite sandstone C4 (b) for three heating–cooling cycles. The course of the expansion curves is indicated by arrows: heat – heating ramp; cool – cooling ramp.

available space to accommodate mismatches of thermal expansion between minerals, and high porosities are related to lower thermal conductivities; on the other hand, low thermal conductivity of stone generates steeper thermal gradients between surface and subsurface, increasing the possibility of thermal expansion mismatches at the surface level, which is more prone to granular disaggregation phenomena through which thermal decay is expressed.

Conclusions

The results of this research show the importance of considering the joint action of different decay factors and the influence of stone properties to explain the differential durability of building stones. Although the statistical analysis shows that the highest correlation is between hygric expansion and decay, expressed as weight loss, this relation does not explain fully why some of the studied materials are less durable than others.

The samples show a series of characteristics suggesting that thermal processes cooperate with hygric expansion to enhance decay. In addition, mineralogical and textural heterogeneity are shown to be one of the main factors contributing to the decay of sedimentary building stones. This can be through the modification of hygric swelling properties that minerals, such as clays, introduce in stone or through enhancing the thermal expansion mismatch of mineral grains. Hygric swelling is modified locally by the presence of clays, which contribute to generate local stresses that, in turn, contribute to increased breakdown of the samples. The probability of thermal-related decay processes increases with the heterogeneity of the stone. Therefore, clay-containing heterogeneous stones show the lowest degree of durability, while clay-free homogeneous siliceous stones show the highest durability.

These results are in agreement with observations made in the built environment in which the localized presence of clays and/or mineral heterogeneities has been reported as major factors triggering and enhancing stone decay (*e.g.* Warke & Smith, 2000; Veniale *et al.*, 2001; Smith *et al.*, 2002; Franzini *et al.*, 2007).

The complexity of the relations between durability and mineralogy, hygric and thermal expansion highlights the importance of studies on the combination of decay factors in understanding the whole context of stone decay. The results of durability tests fail to make sense if they are interpreted in relation to a single decay factor. It is only when considering the combination of agents, and the relations between the stone properties and the environment, that we get meaningful interpretations of durability tests which can be applied to the natural environment. This is especially the case when considering decay factors that are inherently associated in natural environments, which is the case of temperature and humidity.

These results also reflect the importance of considering different scales when studying stone decay. Hygric and thermal expansion operate in different temporal and spatial scales. The stresses generated by the mismatch of thermal expansion rates operate mainly at the grain scale and in the long term. Therefore, the consideration of bulk thermal expansion is not as important as the consideration of the processes that the stone undergoes at the grain scale.

Acknowledgements: This study was funded by the Generalitat Valenciana (Spain) through the Research Project GV05/129. The authors want to express their extreme gratitude to Dr. A. Rodríguez-Guerrero, for his valuable help in measurements of thermal conductivity of stone samples, and K.R. Dotter, for her comments on the manuscript.

References

Aires Barros, K. (2002): Modes and mechanisms of rock weathering. *in* "Protection and conservation of the cultural heritage of the Mediterranean cities", Galán, Zezza, eds. Balkema Publishers, 3-9.

Anon., (1999): Métodos de ensayo para piedra natural. Determinación de la resistencia a la compresión. UNE-EN 1926.

Arpon, R., Molina, J.M., Saravanan, R.A., Garcia-Cordovilla, C., Louis, E., Narciso, J. (2003): Thermal expansion behaviour of aluminium/SiC composites with bimodal particle distributions. *Acta Mater.*, **51**, 3145-3156.

Benavente, D., Lock, P., García-del-Cura, M.A., Ordóñez, S. (2002): Predicting the capillary imbibition of porous rocks from microstructure. *Transport Porous Med.*, **49**, 59-76.

Benavente, D., Cueto, N., Martínez-Martínez, J., García-del-Cura, M.A., Cañaveras, J.C. (2007a): Influence of petrophysical properties on the salt weathering of porous building rocks. *Environ. Geol.*, **52**, 197-206.

Benavente, D., Martínez-Martínez, J., Cueto, N., García-del-Cura, M.A. (2007b): Salt weathering in dual-porosity building dolostones. *Eng. Geol.*, **94**, 215-226.

Bruton, G. (1955): Vapour glycolation. *Am. Mineral.*, **40**, 124-126.

Christensen, N.I. (1990): Seismic velocities. *in* ''Practical handbook of physical properties of rocks and minerals'', R.S. Carmichael, ed. CRC Press, Boca Raton, Florida, 429-546.

Delgado Rodrigues, J. (2001): Evaluación del comportamiento expansivo de las rocas y su interés en conservación. *Mater. Construcc.*, **51**, 183-195.

Dullien, F.A.L., El-Sayed, M.S., Batra, V.K. (1977): Rate of capillary rise in porous media with nonuniform pores. *J. Colloid Interf. Sci.*, **60**, 497-506.

Eeckhout, E.M. (1976): The mechanisms of strength reduction due to moisture in coal mine shales. *Int. J. Rock Mech. Min. Sci. Geomech. Abstr.*, **13**, 61-67.

Fort, R., Bernabéu, A., García-del-Cura, M.A., De Azcona, M.C., Ordóñez, S., Mingarro, F. (2002): Novelda Stone: widely used within the Spanish architectural heritage. *Mater. Construcc.*, **52**, 19-32.

Franzini, M., Leoni, L., Lezzerini, M., Cardelli, R. (2007): Relationship between mineralogical composition, water absorption and hygric dilatation in the ''Macigno'' sandstones from Lunigiana (Massa, Tuscany). *Eur. J. Mineral.*, **19**, 113-123.

Garrecht, H., Hörenbaum, W., Müller, H.S. (1996): Untersuchungen zur Schädigung von witterungsbeanspruchtem Mauerwerk und Folgerungen für die Bausanierung. *in* ''Proc. 4. Internationales Kolloquium Werkstoffwissenschaften und Bauinstandsetzung'', F. H. Wittmann, & A. Gerdes, eds. Esslingen, Germany, 847-860.

Gómez-Heras, M. (2006): Procesos y formas de deterioro térmico en piedra natural del patrimonio arquitectonico, UCM, Servicio de Publicaciones, Madrid, http://www.ucm.es/BUCM/tesis/geo/ucm-t28551.pdf. Last access 15/10/07.

Gómez-Heras, M., Smith, B.J., Fort, R. (2006): Surface temperature differences between minerals in crystalline rocks: implications for granular disaggregation of granites through thermal fatigue. *Geomorphology*, **78**, 236-249.

Gómez-Heras, M. & Fort, R. (2007): Patterns of halite (NaCl) crystallisation in building stone conditioned by laboratory heating regimes. *Environ. Geol.*, **52**, 239-247.

Guéguen, Y. & Palciauskas, V. (1994): Introduction to the physics of rock, Princeton University Press, Princeton.

Halsey, D.P., Mitchell, D.J., Dews, S.J. (1998): Influence of climatically induced cycles in physical weathering. *Q. J. Eng. Geo.*, **31**, 359-367.

Hammecker, C. & Jeannette, D. (1994): Modelling the capillary imbibition kinectics in sedimentary rocks: role of petrographical featrures. *Transport Porous Med.*, **17**, 285-303.

Hower, J. (1961): Some factors concerning the nature and origin of glauconite. *Am. Mineral.*, **46**, 313-334.

Jiménez-González, I. & Scherer, G.W. (2004): Effect of swelling inhibitors on the swelling and stress relaxation of clay bearing stones. *Environ. Geol.*, **46**, 364-377.

Jiménez-González, I., Rodríguez-Navarro, C., Scherer, G.W. (2008): The role of clay minerals in the physico-mechanical deterioration of ornamental stone. *J. Geophys. Res. – Earth Surf.* doi: 10.1029/2007JF000845.

Koch, A. & Siegesmund, S. (2004): The combined effect of moisture and temperature on the anomalous expansion behaviour of marble. *Environ. Geol.*, **46**, 350-363.

Kühnel, R.A. (2002): Driving forces of rock degradation. *in* ''Protection and conservation of the cultural heritage of the Mediterranean cities'' Galán, Zezza, eds. Balkema Publishers, 11-17.

Martín Ramos, J.D. (2004): XPowder, a software package for powder X-ray diffraction analysis. Legal Deposit GR 1001/04.

McCabe, S., Smith, B.J., Warke, P.A. (2007a): Preliminary observations on the impact of complex stress histories on sandstone response to salt weathering: laboratory simulations of process combinations. *Environ. Geol.*, **52**, 269-276.

McCabe, S., Smith, B.J., Warke, P.A. (2007b): Sandstone response to salt weathering following simulated fire damage: a comparison of the effects of furnace heating and fire. *Earth Surf. Proc. Land.*, **32**, 1874-1883.

Moore, D.M. & Reynolds, R.C. (1989): X-ray diffraction and the identification and analysis of clay minerals. Oxford University Press, Oxford, 322p.

Mosquera, M.J., Rivas, T., Prieto, B., Silva, B. (2000): Capillary rise in granitic rocks: interpretation of kinetics on the basis of pore structure. *J. Colloid Interf. Sci.*, **222**, 41-45.

Molina, J.M., Narciso, J., Weber, L., Mortensen, A., Louis, E. (2008): Thermal conductivity of Al–SiC composites with monomodal and bimodal particle size distribution. *Mat. Sci. Eng. A – Struct.*, **480**, 483-488.

Nicholson, D.T. (2001): Pore properties as indicators of breakdown mechanisms in experimentally weathered limestones. *Earth Surf. Proc. Land.*, **26**, 819-838.

Olivier, H.J. (1979): New engineering-geological rock durability classification. *Eng. Geol.*, **14**, 255-279.

Pejon, O.J. & Zuquette, L.V. (2002): Analysis of cyclic swelling of mudrocks. *Eng. Geol.*, **67**, 97-108.

Price, C.A. (1996): Stone conservation. An overview of current research, Getty Conservation Institute, Los Angeles.

Prikryl, R., Svobodová, J., Zák, K., Hradil, D. (2004): Anthropogenic origin of salt crusts on sandstone sculptures of Prague's Charles Bridge (Czech Republic): evidence of mineralogy and stable isotope geochemistry. *Eur. J. Mineral.*, **16**, 609-618.

Sanchez-Moral, S., Luque, L., Cuezva, S., Soler, V., Benavente, D., Laiz, L., Gonzalez, J.M., Saiz-Jimenez, C. (2005): Deterioration of building materials in Roman catacombs: the influence of visitors. *Sci. Total. Environ.*, **349**, 260-276.

Seedsman, R.W. (1993): Comprehensive rock engineering. *in* ''Characterizing Clay Shales'', vol. 3, John A. Hudson, ed. Pergamon Press, Australia, chapter 7, 151-164.

Sebastián, E., Cultrone, G., Benavente, D., Linares, L., Elert, K., Rodríguez-Navarro, C. (2008): Swelling damage in clay-rich sandstones used in the church of San Mateo in Tarifa (Spain). *J. Cult. Herit.*, **9**, 66-76.

Smith, B.J. (1977): Rock temperature measurements from the northwest Sahara and their implications for rock weathering. *Catena*, **4**, 41-63.

Smith, B.J., Turkington, A.V., Warke, P.A., Basheer, P.A.M., McAlister, J.J., Meneely, J., Curran, J.M. (2002): Modelling the rapid retreat of building sandstones: a case study from a polluted maritime environment. *in* ''Natural stone, weathering phenomena, conservation strategies and case studies'', S. Siegesmund, T.N. Weiss, A. Vollbrecht, eds. Geological

Society Special Publication, Geological Soc Publishing House, Bath, 347-362.

Tiab, D. & Donaldson, E.C. (1996): Petrophysics: theory and practice of measuring reservoir rock and fluid transport properties, Gulf Publishing Company, Houston, Texas.

Veniale, F., Setti, M., Rodríguez-Navarro, C., Lodola, S. (2001): Role of clay constituents in stone decay processes. *Mater. Construcc.*, **51**, 163-182.

Warke, P.A. & Smith, B.J. (2000): Salt distribution in clay-rich weathered sandstone. *Earth Surf. Proc. Land.*, **25**, 1333-1342.

Weiss, T., Siegesmund, S., Kirchner, D., Sippel, J. (2004): Insolation weathering and hygric dilatation: two competitive factors in stone degradation. *Environ. Geol.*, **46**, 402-413.

Zimmerman, R.W. & Bodvarsson, G. (1991): A simple approximate solution for horizontal infiltration in a Brooks-Corey medium. *Transport Porous Med.*, **6**, 195-205.

Received 3 December 2007
Modified version received 16 April 2008
Accepted 30 May 2008